Three-Dimensional Vortex-Body Interaction In a Viscous Fluid

FINAL PROGRESS REPORT

JEFFREY S. MARSHALL

July 30, 1999

U.S. ARMY RESEARCH OFFICE
Grant Number DAAH04-96-1-0081

THE UNIVERSITY OF IOWA

SF 298 MASTER COPY KEEP THIS COPY FOR REPRODUCTION PURPOSES

REPORT DOCUMENTATION PAGE

Form Approved
OMB NO. 0704-0188

1. AGENCY USE ONLY *(Leave blank)*	2. REPORT DATE	3. REPORT TYPE AND DATES COVERED
	July 31, 1999	Final Report, 6/1/96 - 7/30/99

4. TITLE AND SUBTITLE

Three-Dimensional Vortex-Body Interaction in a Viscous Fluid

5. FUNDING NUMBERS

DAAH04-96-1-0081

6. AUTHOR(S)

Jeffrey S. Marshall

7. PERFORMING ORGANIZATION NAMES(S) AND ADDRESS(ES)

The University of Iowa
Iowa Institute of Hydraulic Research
Iowa City, Iowa 52242

8. PERFORMING ORGANIZATION REPORT NUMBER

9. SPONSORING / MONITORING AGENCY NAME(S) AND ADDRESS(ES)

U.S. Army Research Office
P.O. Box 12211
Research Triangle Park, NC 27709-2211

10. SPONSORING / MONITORING AGENCY REPORT NUMBER

34934.13-EG

11. SUPPLEMENTARY NOTES

The views, opinions and/or findings contained in this report are those of the author(s) and should not be construed as an official Department of the Army position, policy or decision, unless so designated by other documentation.

12a. DISTRIBUTION / AVAILABILITY STATEMENT

Approved for public release; distribution unlimited.

12 b. DISTRIBUTION CODE

13. ABSTRACT *(Maximum 200 words)*

An experimental and computational study of the impact of a vortex with a body oriented normal to the vortex axis was performed. Particular focus was placed on understanding characteristics of the secondary vorticity ejected from the body and the interaction of the secondary vorticity with the primary vortex. Since both onset of boundary layer separation and the form of the secondary vorticity structures are sensitive to variation of the velocity normal to the body axis, the effect of normal velocity on vortex-body interaction was carefully examined. The physical features of the flow evolution were categorized in terms of an impact parameter and a thickness parameter, which respectively represent ratios of velocity and length scales associated with the vortex to those associated with the flow in the absence of the vortex. Experiments were performed using a combination of laser-induced fluorescence (LIF) flow visualization and particle-image velocimetry (PIV) in a water tank to examine the form of the secondary vorticity structures with both "high" and "low" values of the impact parameter for normal vortex interaction with a circular cylinder and with a thin blade. A new type of Lagrangian vorticity method based on a tetrahedral mesh was developed and applied to compute the secondary vorticity evolution during vortex-cylinder interaction. Computations were also performed for model problems to examine in detail wrapping of a vortex loop around a columnar vortex and impulsive cutting of a columnar vortex with finite axial flow.

14. SUBJECT TERMS			15. NUMBER IF PAGES
			16. PRICE CODE
17. SECURITY CLASSIFICATION OR REPORT	18. SECURITY CLASSIFICATION OF THIS PAGE	19. SECURITY CLASSIFICATION OF ABSTRACT	20. LIMITATION OF ABSTRACT
UNCLASSIFIED	UNCLASSIFIED	UNCLASSIFIED	UL

TABLE OF CONTENTS

LIST OF FIGURES

THREE-DIMENSIONAL VORTEX-BODY INTERACTION IN A VISCOUS FLUID

1. Statement of the Problem

The problem studied in this project involves the impingement of a vortex onto a body in a viscous fluid, where the body travels relative to the vortex in a direction normal to the vortex axis, as shown in figure 1. This problem is commonly referred to in the literature as *normal vortex-body interaction.* The primary application of this research is in the area of helicopter interactional aerodynamics, where it is common for the main rotor wake vortices to impinge on the vehicle fuselage, empennage or tail sections in low speed flight or hover. The research is also applicable to problems associated with ingestion of atmospheric turbulence into the helicopter main rotor.

The simplest model of vortex-blade interaction is that of an infinitesimally thin vortex filament impinging on a body (say, a cylinder) of thickness D, where the vortex filament wraps around the cylinder and comes progressively closer to the cylinder surface as time advances. Letting b denote the minimum separation distance between the vortex filament and the cylinder surface, the cylinder surface pressure would exhibit a $1/b^2$ singularity and the force exerted on the cylinder by the vortex would exhibit a $1/b$ singularity as the vortex approaches the cylinder surface. This singularity is clearly non-physical; it is an artifact of the assumption in the model that all of the vorticity is concentrated on a curve.

There are many ways to regularize this singularity in the context of inviscid theory. For instance, the vortex can be given a finite core area, which might be allowed to change size due to axial stretching or to deform in shape under the influence of the image vorticity. Such modifications to the inviscid theory will produce results that remain bounded during the vortex impact onto the body and may in select cases even yield results for certain parameters consistent with experimental findings. However, detailed experimental and computational investigation of the fluid physics during vortex interaction with bluff bodies in the current study indicates that these refinements to the inviscid theory are generally of secondary importance and do not capture the principal physical processes governing the interaction as the vortex approaches close to the body

surface. In particular, it is found in nearly all cases studied that the secondary vorticity ejected from the body surface interacts strongly with the primary vortex, in some cases causing either complete or partial vortex breakup, prior to actual impact on the body surface. Accurate modeling of the ejected secondary vorticity and its interaction with the primary vortex is thus of critical importance in determining the body surface pressure field and maximum vortex-induced force, both because of the direct influence of the secondary vorticity on the body surface pressure (which can sometimes be substantial) and because of the role of the secondary vorticity in modifying the primary vortex. One exception to this observation occurs for the case of impact of a vortex with a thin blade at sufficiently high normal velocity that the blade boundary layer does not have a chance to separate prior to impact with the vortex.

Normal vortex-body interaction is governed by four dimensionless parameters: the *impact parameter* $I \equiv 2\pi\sigma U/\Gamma$, the *thickness parameter* $T = D/\sigma$, the *axial flow parameter* $A = 2\pi\sigma w_0/\Gamma$, and the *vortex Reynolds number* $\mathrm{Re} = \Gamma/\nu$. Here U is the normal free-stream velocity relative to the body, Γ and σ are the strength and core radius of the primary vortex, w_0 is the average axial velocity in the vortex core, and ν is the fluid kinematic velocity. The primary focus of the current study was to examine the effect of the impact parameter I on the generation, ejection from the body and subsequent evolution of the secondary vorticity field. This study was performed using a combination of several different techniques. An experimental study was performed, using PIV and two-color LIF flow visualization, of vortex interaction with a circular cylinder and a thin blade, in which the parameters A, T, and Re were held fixed while the impact parameter I was varied. An experimental study was also performed for vortex interaction with a fixed sphere, at different distances from the vortex and for spheres of different diameters, in order to understand the effect of a body wake on interaction with a vortex. The results of these experimental studies are summarized in section 2a of this report. Computational studies were performed to examine in detail specific aspects of the flow physics observed during the vortex-body interaction problem. In one such study, the interaction of an initially columnar vortex with a vortex loop was computed, where the vortex loop was used to model a secondary vortex structure after ejection from the body. In another study, the response of a columnar vortex with non-zero axial flow to impulsive cutting by a flat plate was investigated. This study provided insight on the core thinning and thickening near the body and the upstream-propagating waves observed experimentally when a vortex is chopped by a thin blade moving at sufficiently high speed that secondary vorticity does not have a chance to separate from the blade prior to impact with the

vortex. The results of these model studies are described in sections 2b and 2c of this report. Finally, viscous flow computations were performed of normal vortex interaction with a circular cylinder, which fully resolve the generation of secondary vorticity in the cylinder boundary layer, its ejection from the body, and the development and evolution of the shed secondary vorticity structure as it wraps around the primary vortex. These direct computations are performed for different free-stream velocities, oriented both normal and tangential to the cylinder axis. The results of the direct simulation study are described in section 2d of this report.

2. Summary of Results

2a.) Experimental Results for Normal Vortex Interaction with a Body

Experiments were performed involving the interaction in water of a vertical intake vortex with a towed body. The bodies considered in this study include a circular cylinder, a blade at zero angle of attack, and spheres of different diameters. The intake vortex is formed by tangential jets placed at the top of a cylindrical inner tank, measuring $1.3\,m$ high and $0.3\,m$ diameter. The cylindrical tank has a lid, and the vortex is trapped above by an inverted funnel with an optical port in the center. The water is drawn out of the tank through an orifice at the tank bottom. The flow field in the mid-section of the cylindrical tank, at the height of the towed body, is nearly perfectly azimuthal. A rectangular outer tank, placed around the inner cylindrical tank, houses the body and tow supports. The vortex azimuthal velocity profile is measured using particle-image velocimetry (PIV) in the horizontal cross-sectional plane. The vertical velocity within the vortex is measured both using PIV and using video recordings of small ($1\,mm$ nominal diameter) neutrally buoyant dye globules that are advected into the vortex core. Flow visualization is performed using laser-induced fluorescent dyes of different colors. The body boundary layer is marked using dye that fluoresces yellow, which is injected in a series of five small ports placed along the leading edge of the body. The vortex is marked using dye that fluoresces red, which is injected into the center of the funnel at the top of the cylindrical tank and carried downward by the vortex axial flow. Visualization is performed using both horizontal and vertical laser sheets (shown in figure 1) and three-dimensional laser volumes.

Experiments with a blade and a circular cylinder examined the effect of impact parameter on the vortex-body interaction by variation of the towing velocity. The most noticeable effect of impact parameter is on the onset of ejection of the body boundary layer from the leading edge of the body. As shown in figure 2 for the case of a circular cylinder, the boundary layer separation occurs very early for cases with low impact parameter, before the body has a chance to significantly influence the vortex. On the other hand, for sufficiently high impact parameters, boundary layer separation is delayed until after the vortex has bent around the body surface.

The onset of boundary layer separation acts to limit the applicability of inviscid prediction methods for the vortex-induced force on the body due to interaction of the vortex with secondary vorticity shed from the body. For instance, predictions of vortex spanwise displacement obtained using an inviscid filament model are compared with experimental data in figure 3. The filament model predictions are given for four values of impact parameter, ranging from a value $I = 0.027$ characteristic of low impact parameter interactions to a value $I = 0.21$ characteristic of high impact parameter interactions. The experimental data is given only for the values $I = 0.027$ and $I = 0.21$. The data points are plotted using a circle for times prior to boundary layer separation and using a triangle for times after boundary layer separation. Both cases show excellent agreement between the inviscid predictions and the experimental data for times before boundary layer separation and for some period of time just beyond separation. In the low impact parameter case, the experimental data deviate a great deal from the inviscid predictions a short time after boundary layer separation, which illustrates the effect of the secondary vorticity on the vortex location. In the high impact parameter case, the secondary vorticity causes an abrupt breakup of the vortex (at the last data point plotted) shortly after boundary layer separation. For this high impact parameter case, the vortex is already so close to the cylinder at the time of separation that the secondary vorticity is quickly entrained into the vortex core.

We also examined the effect of inviscid deformation of the vortex core shape using computations in which the vortex evolution at high impact parameter is evolved by solution of the full Euler equations (Krishnamoorthy et al. [3]). The computations were performed for high impact parameter ($I = 0.29$) and were stopped at the time at which separation was observed in the experiments. Even when the vortex moves very close to the cylinder (to within about one core radius), the vortex core shape deformation is moderate, with maximum aspect ratio of about 1.5. The slip velocity on the body surface

(and hence the surface pressure) exerted by the deformed vortex is found to be similar to that predicted by the vortex filament model. We therefore believe that the vortex core deformation typically has only slight effect on the vortex-cylinder interaction, except possibly for cases with very high impact parameter. Of course, for cases where the vortex impacts with high impact parameter upon a body with nearly the same dimensions as the vortex core, such as in the computations of vortex impact on a thin blade by Marshall and Grant [11], the inviscid deformation of vortex lines as the body penetrates into the vortex core plays an important role in the vortex cutting process.

The topography of the secondary vorticity structures was examined using flow visualization for vortex interaction with both a cylinder and a thin blade using the vertical and horizontal imaging planes shown in figure 1. For vortex interaction with a cylinder, the boundary layer separation is observed to occur from one location along the cylinder axis, as shown in figure 4a. For vortex interaction with a thin blade, separation occurs along a broad interval over the blade span (figure 4b). For cases with low impact parameter, the secondary vortex structure has the form of a loop that attaches at two points to the cylinder and stretches out to wrap around the primary vortex. A schematic diagram of the secondary vortex loop and a LIF image in the vertical cross-sectional plane *A* are shown in figure 5. For both the case of a thin blade and a circular cylinder, the shed secondary vorticity structures have a loop-like form at low values of the impact parameter; however, the blade sheds a series of loops at different distances from the vortex while the cylinder appears to shed only one loop. For cases with high impact parameter, the secondary vorticity does not separate until after the vortex has wrapped around the front face of the cylinder. Consequently, immediately after separation the secondary vorticity structure has a quasi two-dimensional form that appears to wrap around the primary vortex all along the front face of the body. Shortly after separation, the secondary vorticity impacts on the lateral surface of the primary vortex, giving rise to development of small-scale waves on the lateral surface of the primary vortex core. The secondary vorticity is quickly entrained within the primary vortex core, leading to rapid breakup of the vortex. A schematic diagram of the secondary vorticity and an LIF image in the vertical plane *A* are shown in figure 6.

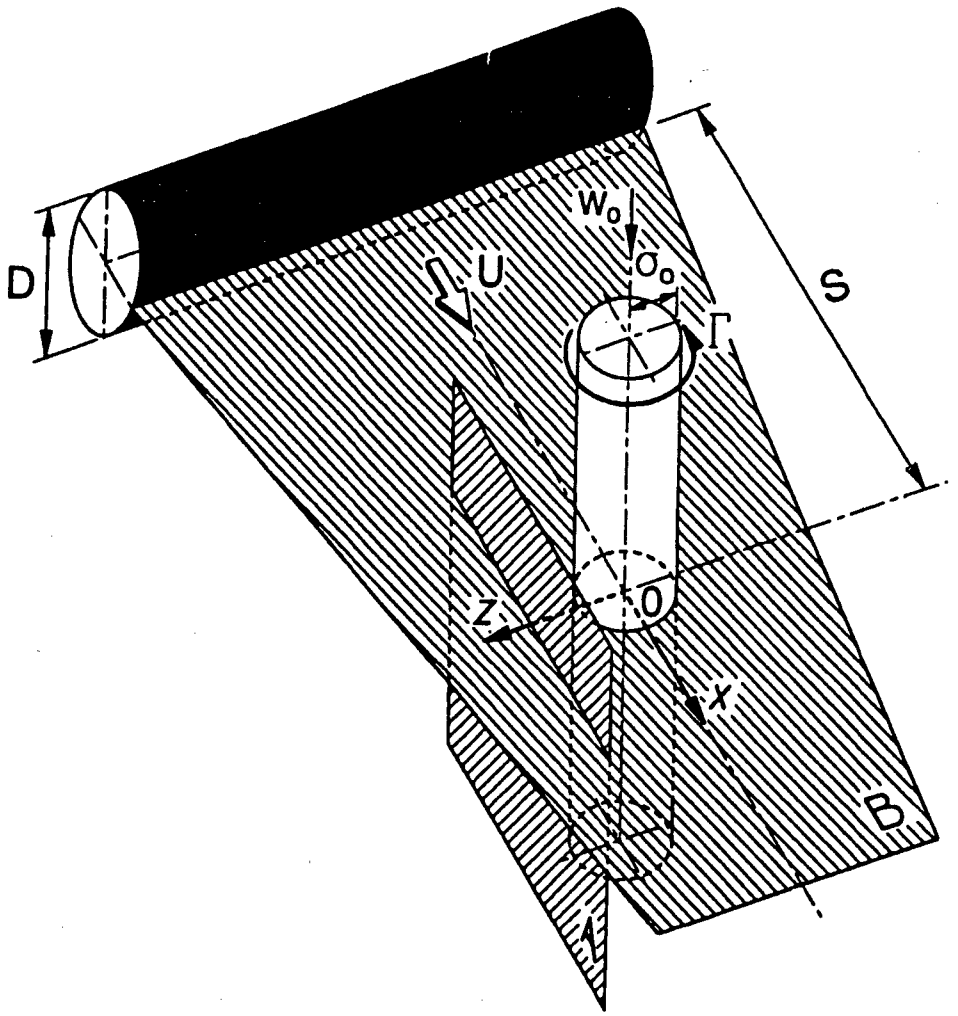

Fig. 1. Sketch illustrating the coordinate system used to measure vortex displacement, various parameters that govern normal vortex-cylinder interaction, and the vertical plane *A* and horizontal plane *B* used for flow visualization [3].

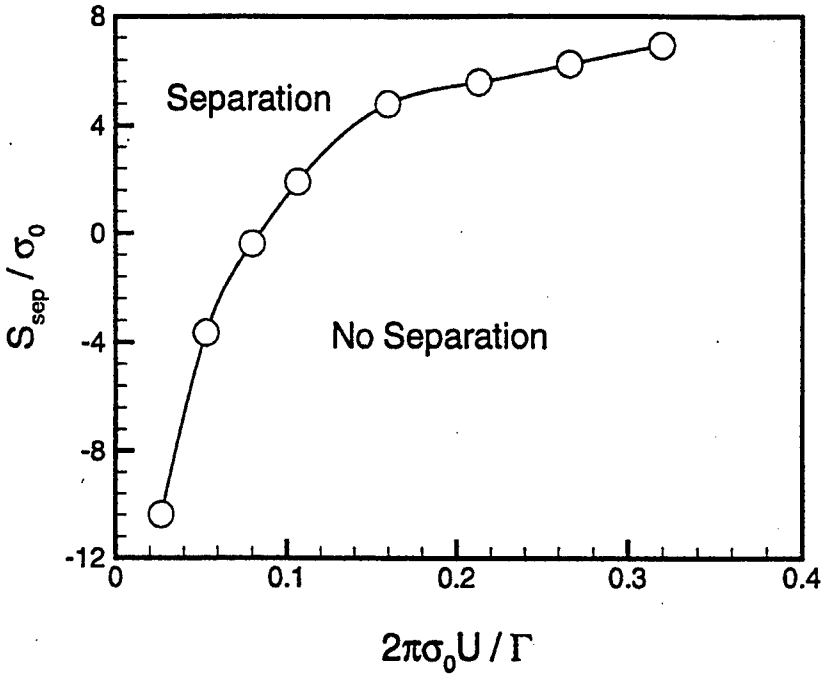

Fig. 2. Experimental data for variation of the critical value of the cylinder leading edge position at the instant of boundary layer separation (S_{sep}) as a function of the impact parameter I [3].

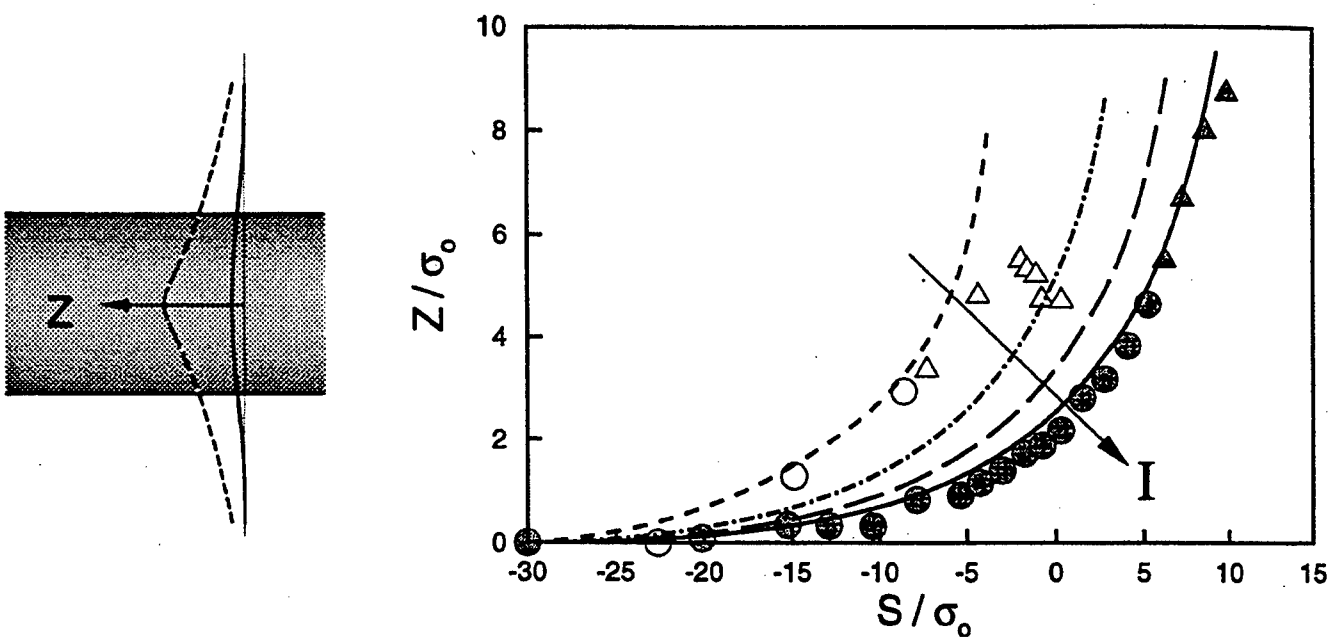

Fig. 3. Results for axial displacement Z of the vortex cross-section in the horizontal plane B during vortex-cylinder interaction, showing filament model predictions with $I = 0.21$ (solid), 0.15 (long dashed), 0.088 (dash-dotted), and 0.027 (short dashed) and experimental data with $I = 0.21$ (open symbols) and 0.027 (shaded symbols). Experimental data points are given for times both before (circles) and after (triangles) boundary layer separation from the cylinder [3].

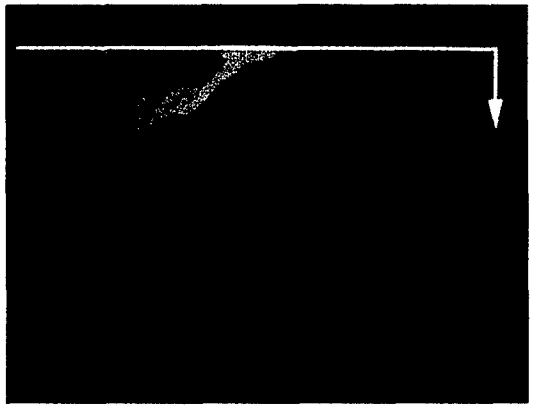

(a) Circular cylinder

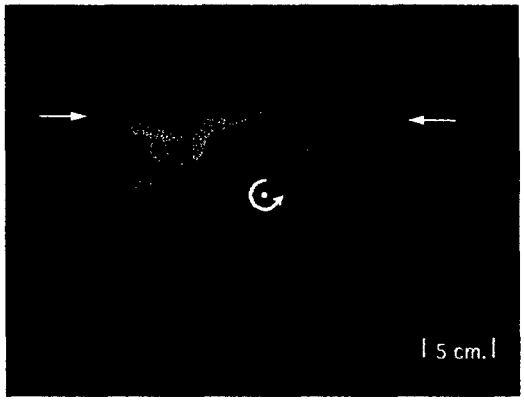

(b) Thin blade

Fig. 4. LIF photographs in the horizontal plane *B* showing onset of boundary layer separation from the body leading edge for (a) a circular cylinder [3] and (b) a thin blade [5].

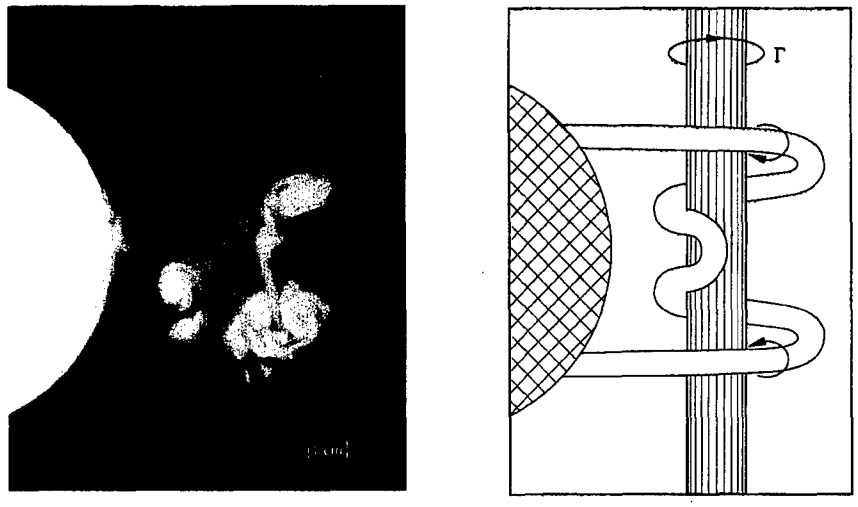

(a) (b)

Fig. 5. Illustration showing a secondary vortex loop (yellow) for a low impact parameter case ($I = 0.027$) as it wraps around the primary vortex (red) for (a) a photograph of an LIF slice in the vertical plane A and (b) a schematic diagram [3].

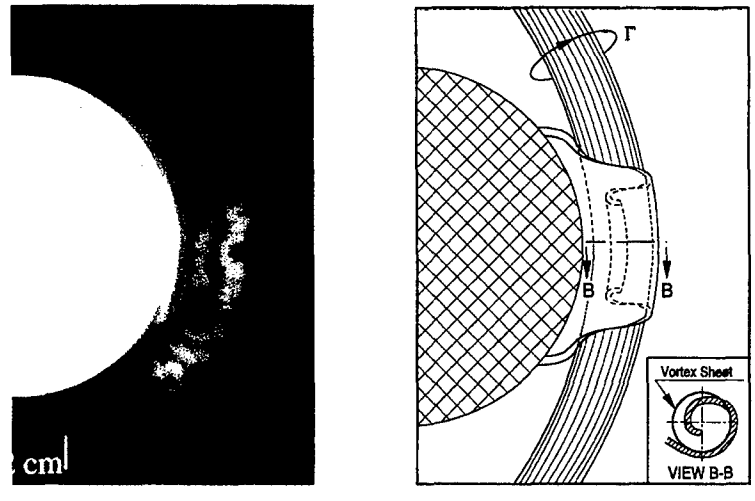

(a) (b)

Fig. 6. Illustration showing wrapping of the secondary vorticity (yellow) about the primary vortex (red) for a high impact parameter case ($I = 0.21$) for (a) a photograph of an LIF slice in the vertical plane A and (b) a schematic diagram [3].

2b.) Computational Results for Effect of Secondary Vorticity on Primary Vortex

After the secondary vorticity is ejected outward from the body, the swirling motion of the primary vortex causes the secondary vorticity to rotate around the primary vortex while the self-induced velocity of the secondary vortex structure causes it to advect inwards toward the primary vortex core. For secondary vorticity ejected while the primary vortex is only a few core radii away from the body leading edge, the secondary vorticity is observed to impact on the lateral core boundary of the primary vortex after only one or two rotations. Experimental observations indicate that the wrapped secondary vorticity can cause abrupt disruptions of the primary vortex, sometimes even triggering a vortex breakdown event. The specific effects of the secondary vorticity have been investigated in more detail using inviscid computations both for an axisymmetric case with rings of secondary vorticity wrapped around a columnar vortex (figure 7a) and for a fully three-dimensional case with a vortex loop wrapping around an initially columnar vortex (figure 7b). The three-dimensional case is representative of the early part of the wrapping process where the nose of the secondary vortex loop first begins to wrap around the primary vortex, while the axisymmetric case is representative of the later stages of the process where the secondary loop has made at least one complete rotation about the primary vortex core. Of principal interest in this computational study is the response of the primary vortex to the forcing exerted by the secondary vortex structures.

One of the most important effects of the induced velocity from the secondary vortex structures is the development of variation in core area of the primary vortex, which takes the form of outward bulging of the core in regions where the vortex is axially compressed and thinning of the core in regions where the vortex is stretched. This bulging and thinning of the core causes radial tilting of the initially axial vortex lines within the primary vortex core. In the presence of the radial variation in angular rotation rate in the outer regions of the primary vortex core, this radial component of vorticity tilts in the azimuthal direction. The net result of the core bulging and thinning process is therefore a build up of azimuthal vorticity within the primary vortex core. As shown in figure 8, the induced azimuthal vorticity within the primary vortex core is located nearly directly below the secondary vorticity structures and has a sign opposite to that of the azimuthal vorticity component of the secondary vorticity structures.

For cases where the secondary vorticity is located periodically along the primary vortex core, the azimuthal vorticity within the primary vortex core acts to induce a

standing wave pattern that resists the change in core area induced by the secondary vortices. When the secondary vortex structures are sufficiently weak compared to the primary vortex, the primary vortex responds to the velocity induced by the secondary structures simply by periodic oscillations in core area. In the case where a single vortex loop is wrapped around the primary vortex, the induced azimuthal vorticity within the vortex core pairs with the secondary vortex structure to advect the legs of the vortex loop in opposite directions along the primary vortex axis. In either of these cases, sufficiently strong secondary vorticity results in formation of a cusp in the bulging part of the primary vortex core, from which vorticity from within the primary vortex is ejected outward in the form of thin sheets. We refer to this latter process as *vorticity stripping*. A sequence of pictures illustrating the development of vorticity ejection from the primary vortex core are given in figure 9 for the case of periodic secondary vortex rings about a columnar vortex. The vorticity stripping process was observed in an earlier experimental study by Sarpkaya and Daly [13], who examined the interaction of a columnar vortex with surrounding turbulence, although the dynamics underlying this process was not at that time appreciated.

The full three-dimensional computations of vortex loop-columnar vortex interaction also exhibit certain uniquely three-dimensional effects, not present in the axisymmetric computations. A plot of an iso-surface of the vorticity magnitude during this interaction is given in figure 10, which shows three-dimensional vorticity ejection from the columnar vortex all around the outside of the vortex loop nose. The velocity induced by the loop nose also causes a pronounced deformation in shape of the columnar vortex cross-section. The development of core shape deformation for the three-dimensional computation of vortex loop interaction with a columnar vortex is shown in a time series in figure 11 for a cross-section in the y-z plane.

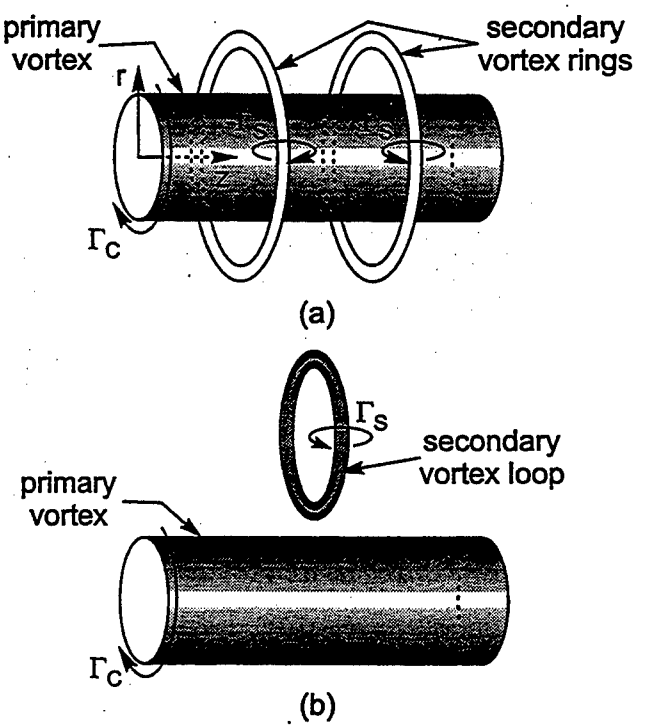

Fig. 7. Schematic diagram showing the initial conditions for computation of the interaction of the primary vortex with wrapped secondary vorticity, for (a) an axisymmetric case and (b) a fully three-dimensional case.

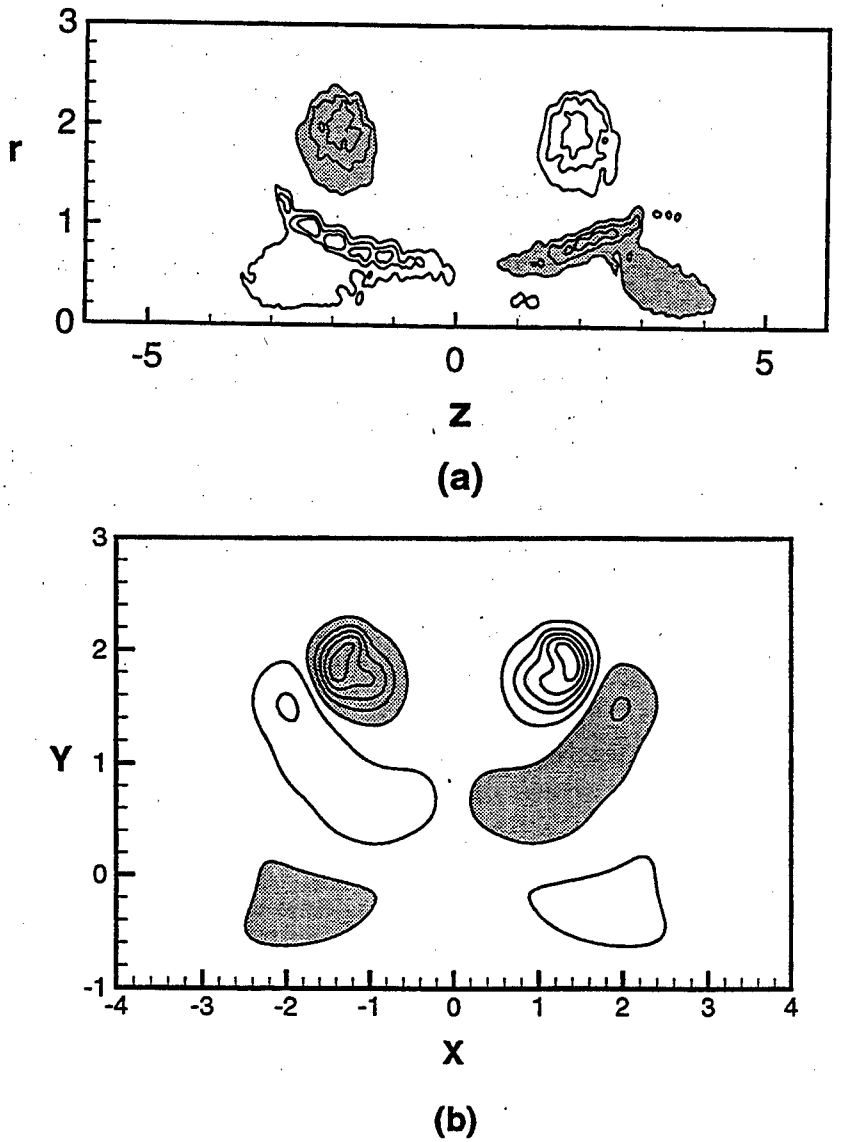

Fig. 8. Contour plots showing the azimuthal vorticity induced within the primary vortex core by wrapped secondary vorticity structures for (a) an axisymmetric case and (b) a fully three-dimensional.

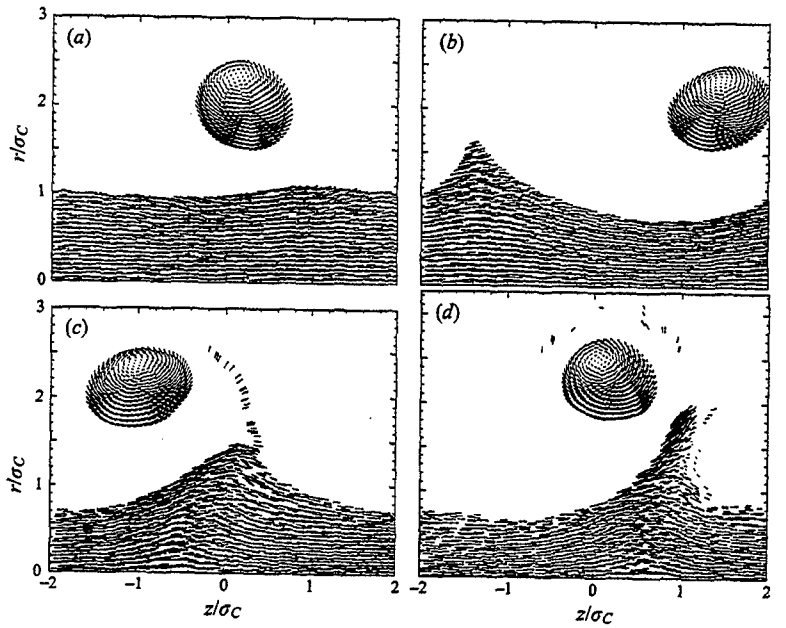

(a) Same sign

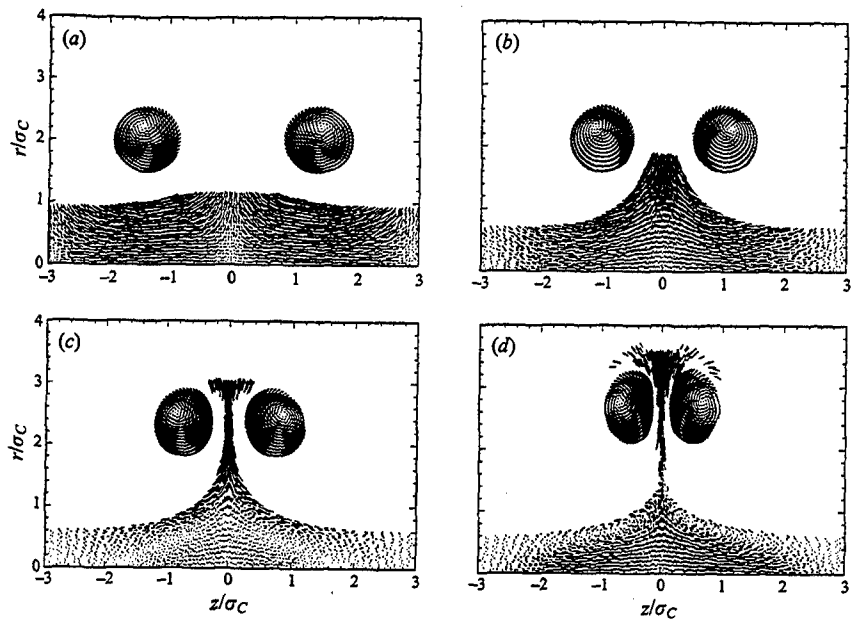

(b) Alternating sign

Fig. 9. Sequence of pictures illustrating the development of ejection of vorticity from the primary vortex core for the case (a) same sign and (b) alternating sign periodic vortex loops encircling a columnar vortex [9].

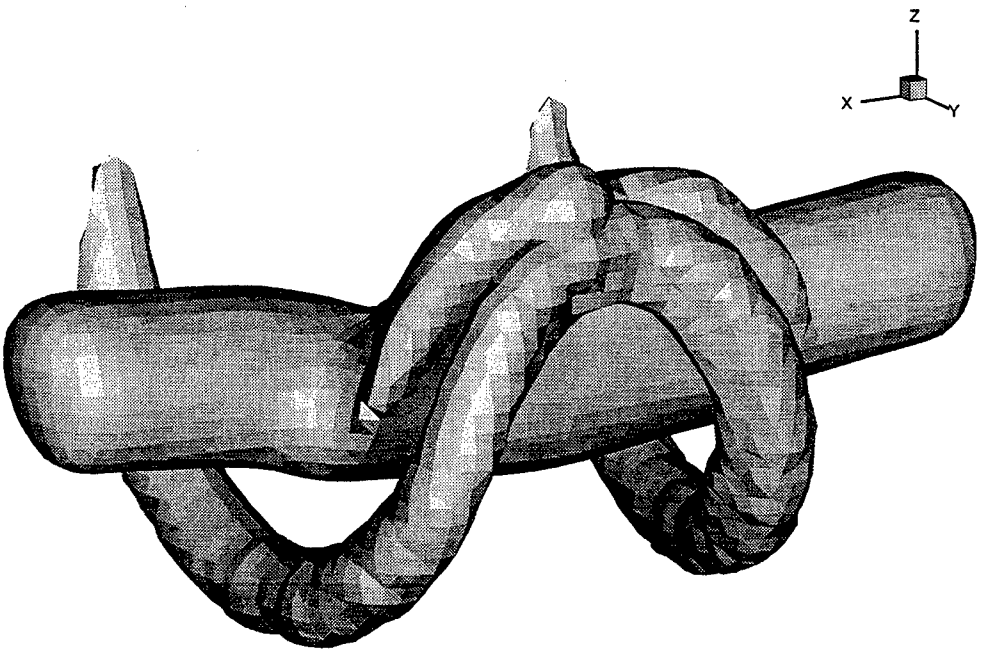

Fig. 10. Iso-surface of vorticity magnitude showing the three-dimensional wrapping of a vortex loop around a columnar vortex [5].

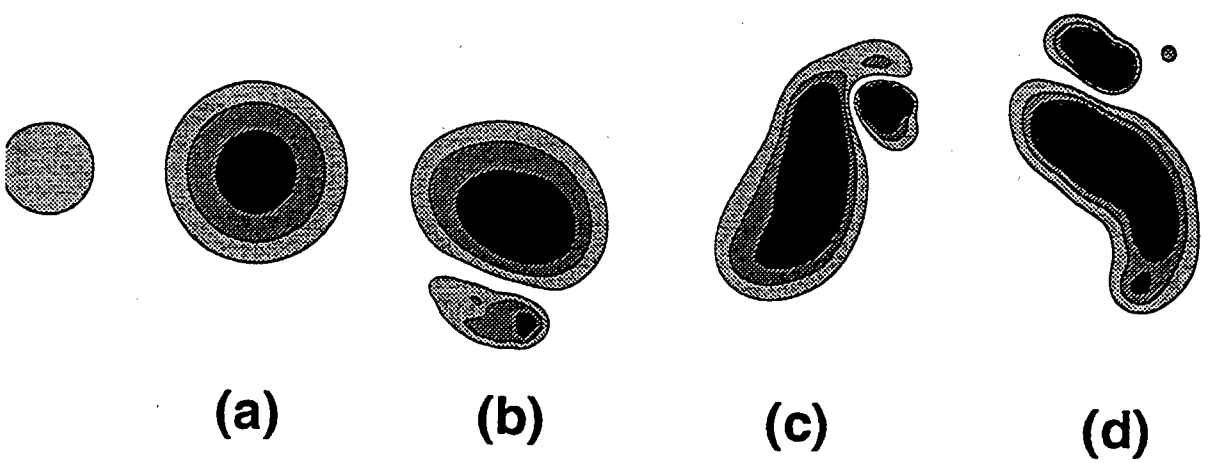

Fig. 11. Series of vorticity contour plots in the y-z plane for the problem illustrated in figure 10, showing the deformation in shape of a cross-section of the columnar vortex core induced by the nose of the vortex loop [5].

2c.) Computational Results for Impulsive Cutting of a Vortex With Axial Flow

When a thin body impacts a vortex core at sufficiently high impact parameter, the body will penetrate into the ambient position of the vortex core prior to separation of the body boundary layer. For an inviscid fluid, the vorticity lines within the vortex core will deform around the body during this penetration, as shown in the inviscid computations of Marshall and Grant [11] (figure 12). In a viscous fluid, cross-diffusion between the body boundary layer vorticity and the deformed vorticity field within the primary vortex will lead to connection of the primary vortex lines to the body boundary layer, resulting in an apparent "cutting" of the vortex. In the case of a vortex with non-zero axial flow, vortex cutting will cause a sudden blockage of the axial velocity field, with subsequent compression of the axial vortex lines in the primary vortex upstream of the body and stretching of the vortex lines downstream of the body.

In order to study the response of a columnar primary vortex with non-zero axial flow to sudden cutting by a thin body, inviscid computations have been performed of an axisymmetric columnar vortex in which the axial velocity is suddenly brought to zero at a given location [10]. The vortex response is found to be quite different for the cases of sub-critical and super-critical vortex flow, where we recall that the critical point corresponds to a state where upstream propagating waves of variable core area are held stationary by the axial velocity within the vortex core. In both cases, a vortex expansion wave is observed downstream of the vortex core propagating away from the body, over which the core radius changes from the ambient value downstream of the wave to a smaller (constant) value upstream of the wave. The expansion wave is typified by a series of azimuthal vortex rings of alternating sign, which propagate downstream from the cutting point.

In the case of a sub-critical vortex, a vortex compression wave is observed on the upstream side of the vortex, which propagates upstream from the cutting body against the ambient axial flow. This compression wave is again associated with a series of rings of azimuthal vorticity of alternating sign, over which the core radius changes from the ambient value upstream of the compression wave to a greater (constant) value in the region in-between the compression wave and the cutting body. Behind both the expansion and compression waves, the radial and axial velocity components of the vortex are brought nearly to zero, so that the vortex is in a state of nearly pure swirl. The existence of the up-stream propagating waves following cutting of a sub-critical vortex have been

verified experimentally by Krishnamoorthy and Marshall [4], Marshall and Krishnamoorthy [10], and Maxworthy, Hopfinger and Redekopp [12]. Flow visualization pictures of these upstream propagating waves which occur following cutting of a sub-critical vortex (figure 13) exhibit bubble- or spiral-type forms that appear similar to flow visualization images of vortex breakdowns observed in other situations, such as in a diverging tube or delta-wing vortices.

For a super-critical vortex, all waves of variable core area are swept downstream by the axial flow, so the vortex response following cutting is to impact the cutting surface with a continuously spreading core, much like a liquid jet impacts a flat plate. Close-up plots showing the vortex response upstream of the cutting surface in both the sub-critical and super-critical cases are shown in figure 14. The super-critical vortex case was also examined by Lee, Burggraf and Conlisk [6], who obtained similar results.

For either sub-critical or super-critical vortex flows, the bulging of core radius upstream and the core thinning downstream of the cutting surface results in a normal force on the body in the direction of the vortex axis. The results from axisymmetric computations for the sub-critical vortex case are compared to the theoretical solution of Marshall [8] using the plug-flow model of Lundgren and Ashurst [7]. This theory is mathematically similar to the gas-dynamics problem of impulsive motion of a piston in a shock tube, with the core radius playing a role similar to the gas density. Table 1 gives a comparison of computational and experimental flow visualization results with the model predictions. The computations are found to compare quite well with the model predictions for the change in core radius and the normal force on the cutting body, while experimental data for propagation speed of the upstream propagating vortex waves are also found to compare well to theoretical predictions for propagation speed of a "vortex shock".

There are several aspects of this problem that require further study, most of which involve viscous flow effects of the vortex interaction with the cutting body. For instance, a detailed study of the actual cutting process is required to examine the extent of vortex line deformation prior to cutting and reconnection of the vortex lines with the boundary layer vorticity. It is observed experimentally that vorticity from the body boundary layer is entrained into the vortex core and propagates axially upstream and downstream from the cutting body. While this entrainment process has been studied for the steady-state case of a vortex over a fixed plate, the effect of plate translation on the vorticity entrainment is

not clear. The effect of axial secondary vorticity entrainment on the primary vortex response also needs to be examined. Perhaps the most important problem in this category has to do with the onset and effects of boundary layer separation from the leading edge of the body as it is in the process of penetrating into the core of the vortex, which occurs due to the impact of the vortex axial flow on the body leading edge. We observe experimentally that secondary vorticity is shed from the body leading edge and is entrained into the primary vortex core. Of particular concern is the question of whether the force induced on the blade by the leading edge vorticity shedding during the initial penetration of the body into the vortex is large or small in magnitude compared to the asymptotic normal force on the body due to the vortex core radius difference.

Comparison Quantity	Axial flow parameter, A	Plug-flow model [8]	Axisymmetric computation	Experiment
Compression wave speed, mm/s	0.15	365		320 ± 5
Asymptotic core radius ratio, $\sigma_{compression} / \sigma_{expansion}$	0.17	1.28	1.29	
Asymptotic value of force on the cutting surface, $F / \rho\Gamma^2$	0.17	-0.020	-0.023	
Asymptotic core radius ratio, $\sigma_{compression} / \sigma_{expansion}$	0.20	1.33		1.4 ± 0.1

Table 1. Comparison of results obtained from plug-flow model [7,8] with results of the direct axisymmetric computation and experiments [10].

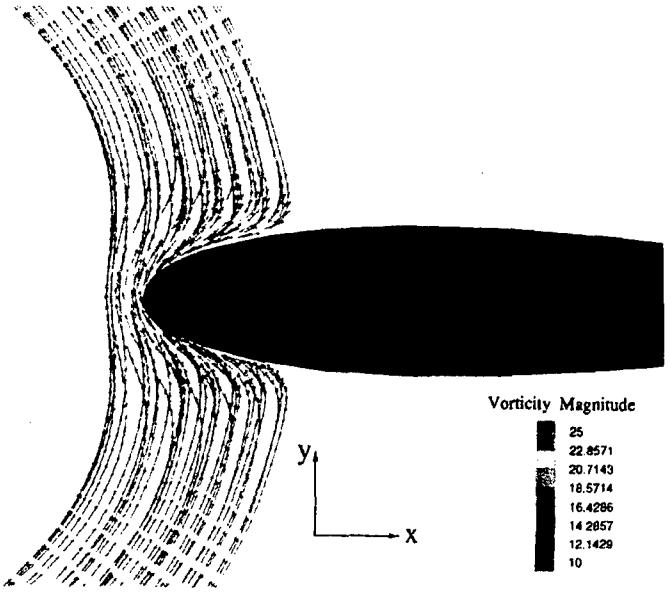

Fig. 12. Deformation of vorticity vectors as a thin blade penetrates into a vortex core in an inviscid fluid [11].

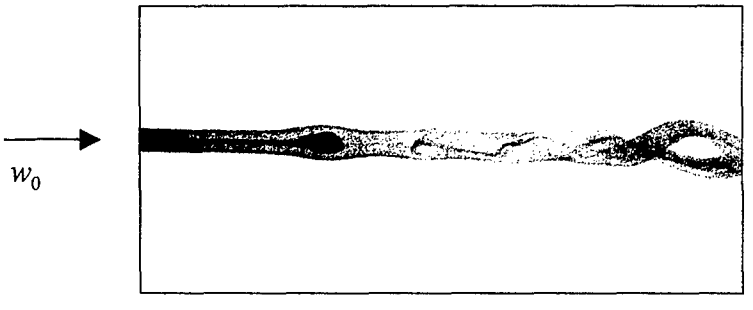

Fig. 13. Flow visualization image of an up-stream propagating vortex wave, which forms immediately following cutting of a vortex by a thin plate [4].

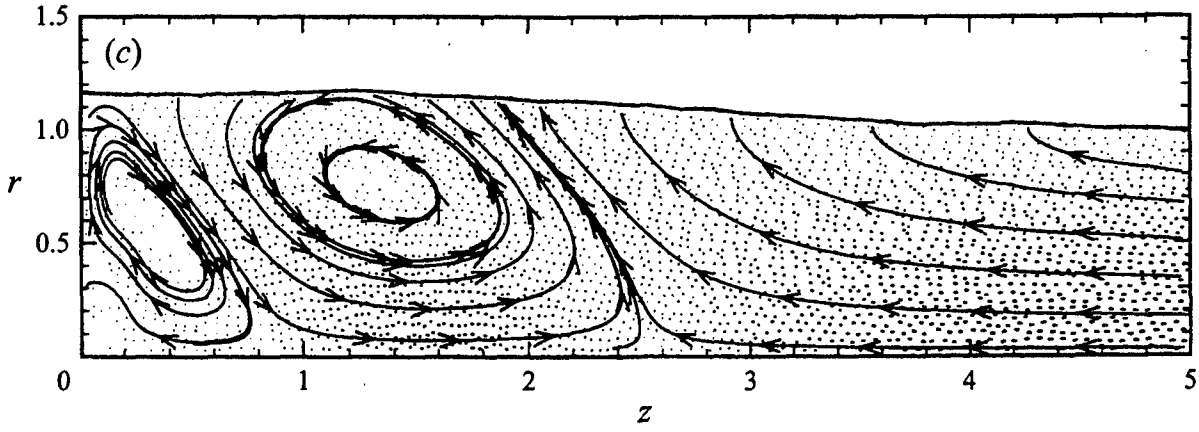

(a) Sub-critical case

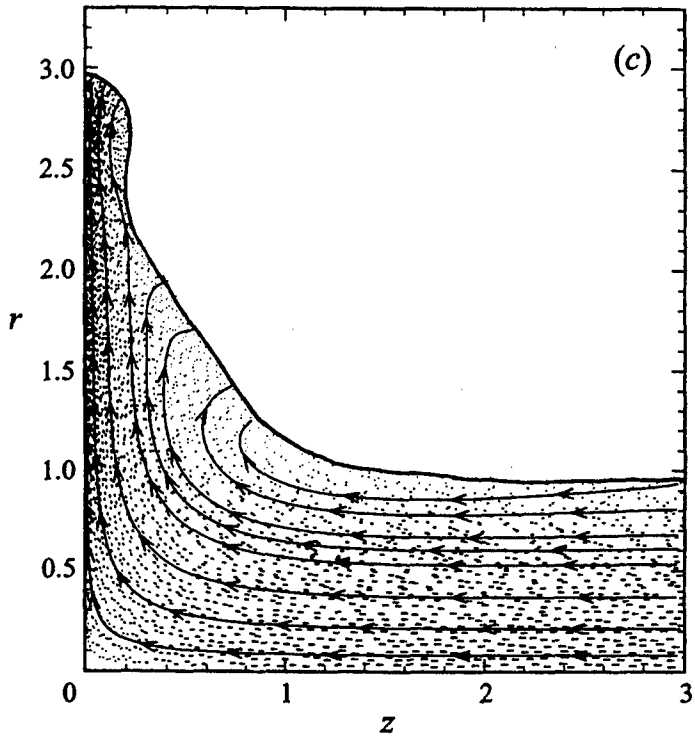

(b) Super-critical case

Fig. 14. Computational results showing the variation of the vortex core upstream of a cutting surface for (a) a sub-critical vortex and (b) a super-critical vortex. The sub-critical vortex develops a wave that propagates upstream on the vortex core, while the super-critical vortex spreads out on the cutting surface much like a liquid jet impinging into a plane wall [10].

2d.) Direct Computation of Vortex-Cylinder Interaction

Direct computation of normal vortex-cylinder interaction was performed for cases with different impact parameters and both with and without free-stream flow tangential to the vortex axis. The computations capture the full viscous response of the body, including development of secondary vorticity in the body boundary layer, outward ejection of secondary vorticity from the body, and wrapping of the secondary vortex structure around the primary vortex. To simplify the computations, the primary vortex is modeled by a vortex filament, where the displacement of the filament in the presence of the body is computed using inviscid theory. The computations are therefore limited to the early stages after the secondary vorticity is ejected from the body, prior to any significant effect of the secondary vorticity on the primary vortex. Based on our experimental observations, we limited the computations to one rotation of the secondary vorticity around the primary vortex.

The computations are performed using a new type of Lagrangian vorticity method, in which a tetrahedral mesh is fit to the advected computational points at every time step and is used to interpolate the vorticity in-between the Lagrangian computational points. The vorticity on each computational point is evolved using the vorticity transport equation and the velocity field is computed using the Biot-Savart integral. A fast multipole expansion method is used to accelerate the Biot-Savart integration. Derivatives in the vortex stretching and diffusion terms of the vorticity transport equation are computed using a moving least-squares algorithm. The body surface pressure is computed using a boundary-integral method based on the Green's function solution. This method possesses all of the advantages of traditional vortex methods, including (1) the need for computational points only in the part of the flow field with significant vorticity, (2) no numerical dissipation, and (3) the computational mesh naturally adapts to the changing vorticity field. However, unlike traditional vortex methods, the tetrahedral vortex element method maintains a sharp vorticity discontinuity at the body surface, without bleeding of vorticity over the surface boundary. Also, the tetrahedral vorticity element method allows for highly anisotropic elements, which are much more efficient than typical vortex methods using isotropic vortex blobs for resolution of thin three-dimensional boundary layers. An improved flux-based method for setting the vorticity boundary conditions on the body has also been developed using the moving least-sqaure differentiation method.

The initial condition and coordinates for the vortex-cylinder interaction computation are shown in figure 15. All variables are non-dimensionalized using the cylinder diameter D and the ratio D^2/Γ as length and time scales, respectively. The different cases examined in the computations are shown in table 2. In this summary, we will particularly discuss cases 2 and 5 in this table. In case 2, the vortex is initiated as a straight line at a distance $d = 0.3$ from the cylinder leading edge, with no background free-stream velocity. The secondary vorticity response in this case is characteristic of normal vortex-cylinder interaction at low values of the impact parameter. In case 5, a free-stream velocity exists normal to the cylinder axis, where the velocity magnitude is set to correspond to the high impact parameter case examined experimentally by Krishnamoorthy, Gossler and Marshall [3]. For this case, the vortex is initialized as a straight line at a distance $d = 1.5$ from the cylinder leading edge, which is chosen based on experimental observations that the vortex bending is negligible before this point. The inviscid vortex filament solution is then carried forth until vortex is separated within about three vortex core radii from the cylinder leading edge, which is used as an initial condition for the boundary layer calculation.

(U_x, U_y, U_z)	Re = 500	Re = 1500
(0,0,0)	**Case 1**	**Case 2**
(0,0,U)	X	**Case 3**
(0,0,–U)	X	**Case 4**
(0,U,0)	X	**Case 5**

Table 2. Summary of computational cases examined.

For the case with no free-stream velocity (case 2), the secondary vorticity is observed to form a loop-like structure that attaches at two points to the cylinder surface and wraps around the primary vortex core. A time series plotting velocity vectors attached to the Lagrangian control points in a thin slice of the flow is given in figure 16, showing the ejection of the secondary vorticity from the body and its wrapping around the primary vortex. An iso-surface of vorticity magnitude showing the loop-like form of the secondary vorticity structure is plotted in figure 17. Streamlines and a vorticity contour plot over a slice of the secondary vortex loop at $y = 0.2$, near the base of the loop-like structure, are given in figure 18. The vorticity contours exhibit two strong vortex legs

with opposite sign vorticity component normal to the page. Streamlines in the y-z plane, which lies directly between the legs of the secondary vortex loop, are plotted in figure 19 for both inviscid and viscous flow cases. The ejection of the secondary vorticity is shown to dramatically modify the flow external to the boundary layer, reversing the flow direction tangent to the cylinder surface in the region above the primary vortex. Limiting surface streamlines and surface vorticity lines are plotted in figure 20. The limiting streamlines exhibit nodes at the point of attachment of the loop legs to the cylinder. A saddle point is located at the midpoint of the separation line stretching between the nodes. The surface vortex lines exhibit foci with rotation of opposite sign at the attachment points of the secondary vortex loop. The surface pressure field is compared for inviscid and viscous flow cases in figure 21. In the inviscid flow case, the surface pressure is nearly symmetric above and below the vortex filament, with a pressure minimum directly under the vortex. This symmetry is broken in the viscous flow case, for which a low pressure region is located near the attachment point of the vortex loop legs with the body.

For the case with free-stream velocity normal to the cylinder axis (case 5), the secondary vorticity forms a vortex with opposite sign to the primary vortex that wraps around the front of the cylinder. The secondary vorticity is ejected radially outward from the cylinder surface in a sheet all along the front face of the cylinder. An iso-surface of vorticity magnitude showing the quasi two-dimensional form of the secondary vortex as it forms a ridge wrapping around the cylinder is given in figure 22. A vorticity contour plot and streamlines over a slice of the secondary vortex structure in the y-z plane are given in figure 23. The streamlines show both the primary vortex and the counter-rotating secondary vortex structure. Limiting surface streamlines and surface vorticity lines are shown in figure 24. The limiting streamlines exhibit a separation line that stretches around the front of the cylinder. The separation line has a saddle at the middle, but no nodes at the endpoints, as were observed for the case without normal free-stream velocity. The surface vortex lines similarly do not exhibit foci at the endpoints of the separation line, as were observed for the case with no free-stream velocity. The surface pressure field is compared for inviscid and viscous flow cases in figure 25. Both the viscous and inviscid cases exhibit a high-pressure region near the stagnation point induced by the vortex filament along the cylinder leading edge, but the pressure magnitude is significantly greater for the viscous case.

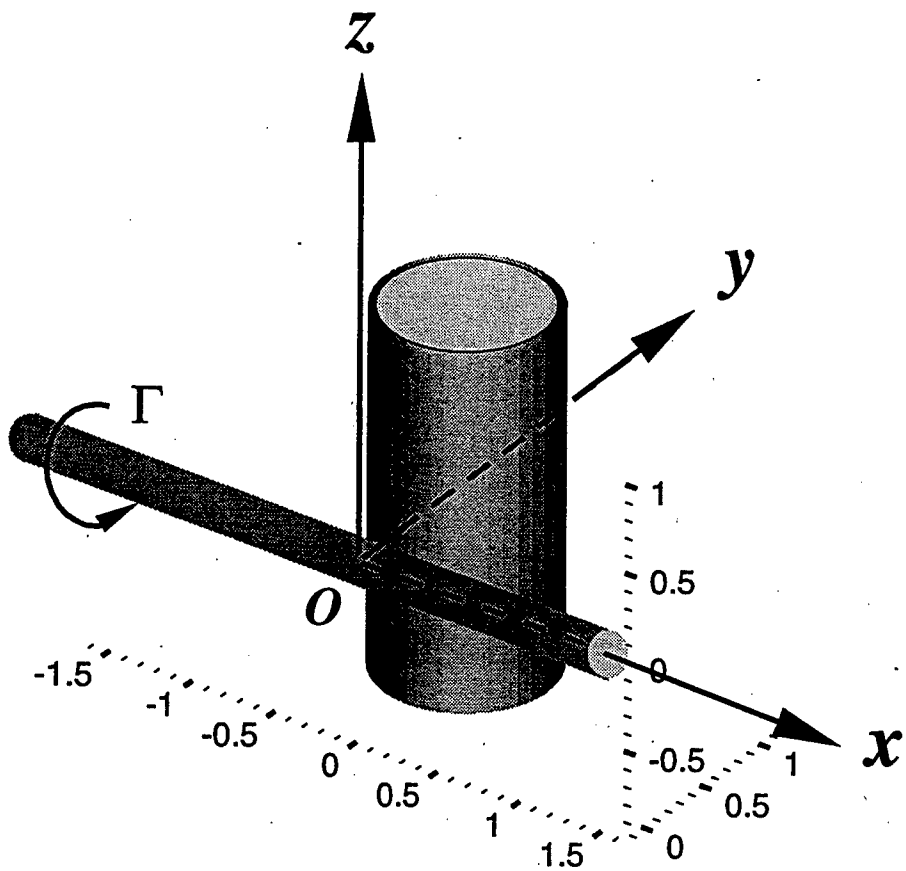

Fig. 15. Initial condition and coordinate system for direct computation of vortex-cylinder interaction [2].

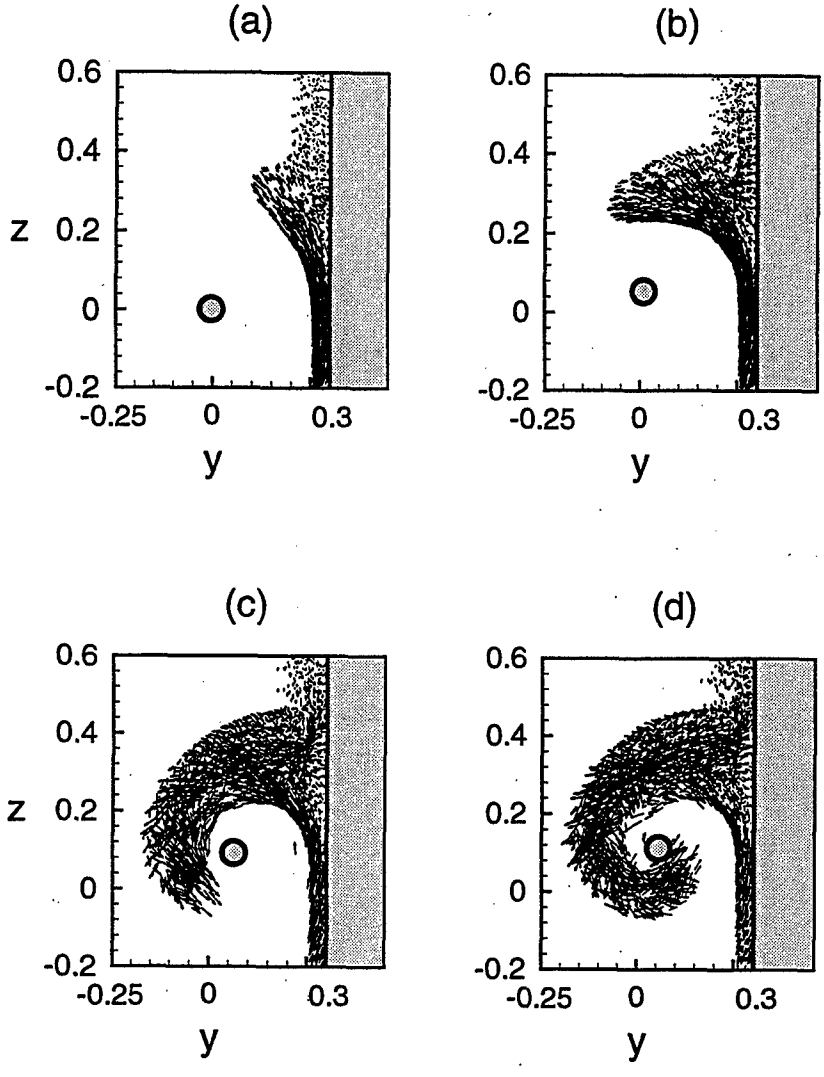

Fig. 16. Velocity vectors attached to Lagrangian vorticity control points in a thin slice of the flow at four times as the secondary vorticity is ejected from the cylinder and wraps around the primary vortex (indicated by a circle) [2].

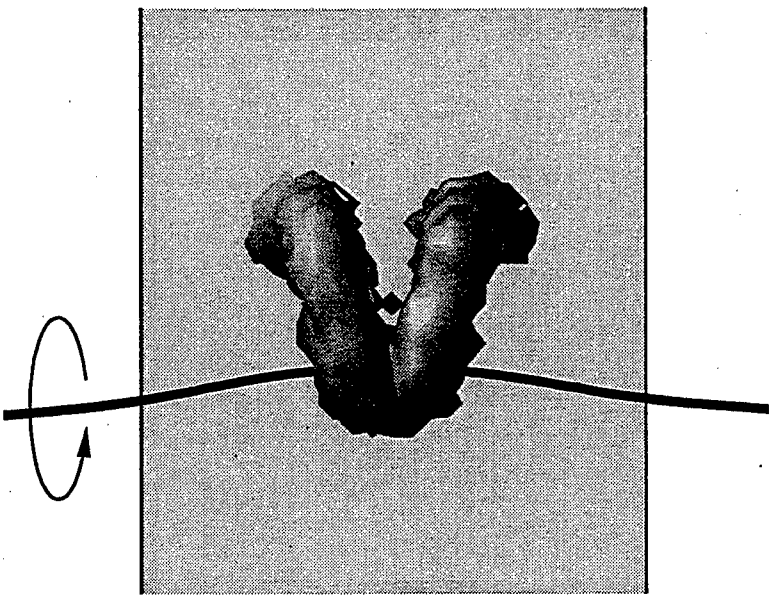

Fig. 17. Iso-surface of vorticity magnitude, showing the loop-like form of the secondary vorticity for the case of no free-stream flow [2].

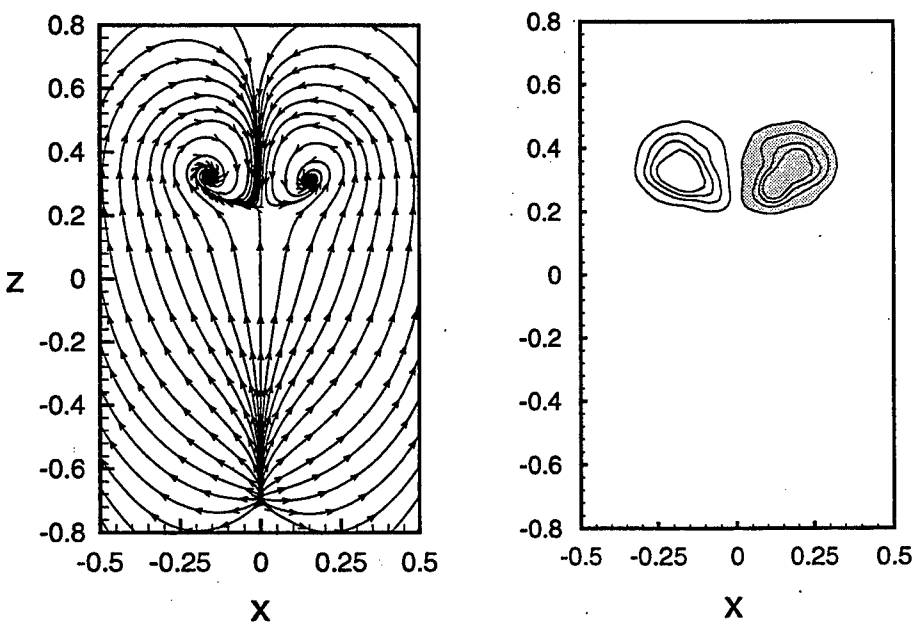

Fig. 18. Streamlines and contour plot of the normal vorticity over a slice of the secondary vortex loop in the plane $y = 0.2$ for the case with no free-stream velocity [2].

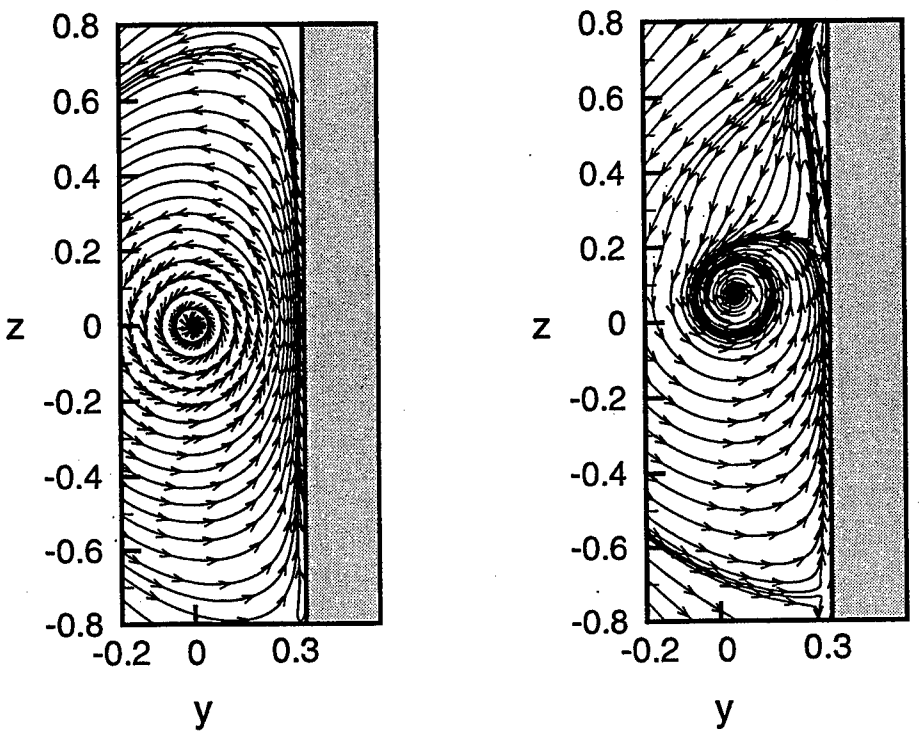

Fig. 19. Streamlines in the y-z plane, bisecting the legs of the secondary vortex loop, for (a) inviscid and (b) viscous flow in the case with no free-stream velocity [2].

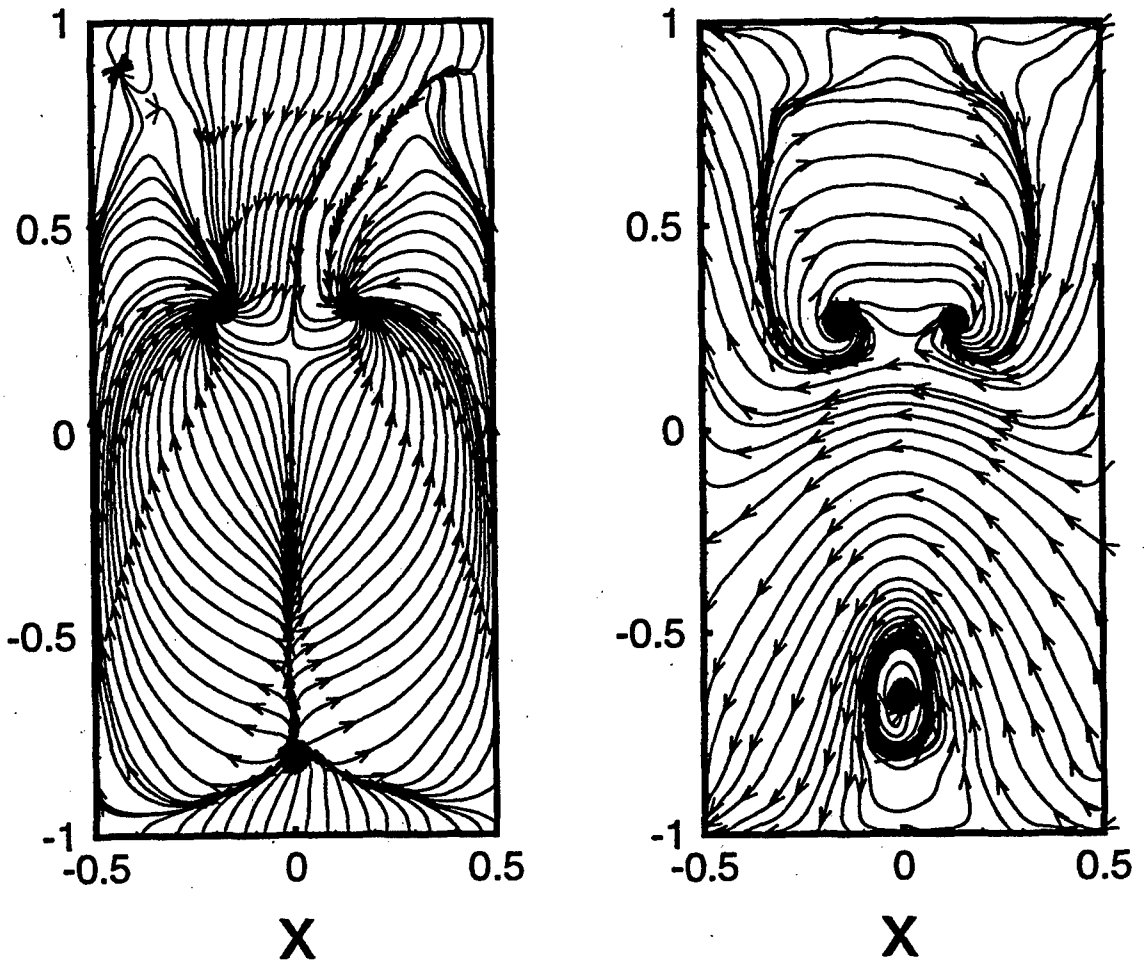

(a) (b)

Fig. 20. Plot of the (a) limiting surface streamlines and (b) surface vortex lines for vortex-cylinder interaction with no free-stream velocity [2].

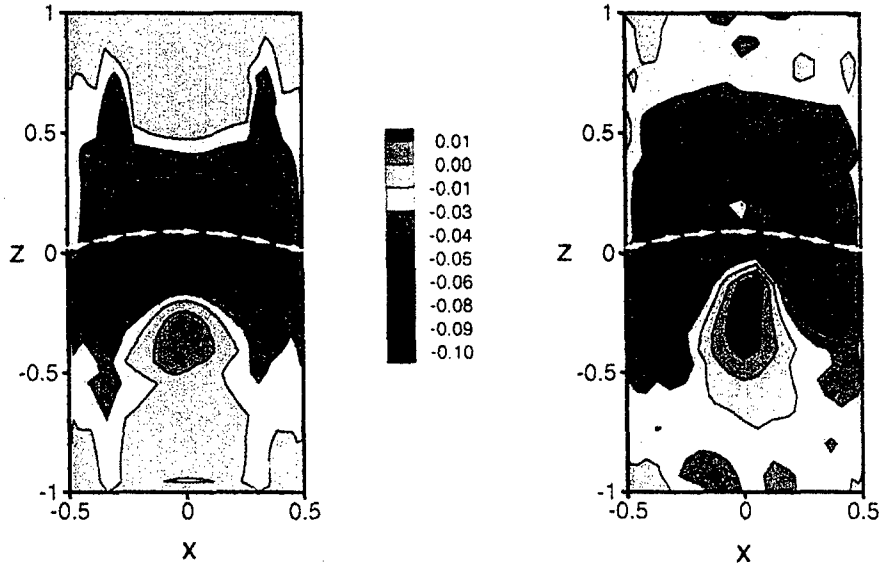

(a) (b)

Fig. 21. Surface pressure for vortex-cylinder interaction with (a) inviscid and (b) viscous flow for a case with no free-stream velocity [2].

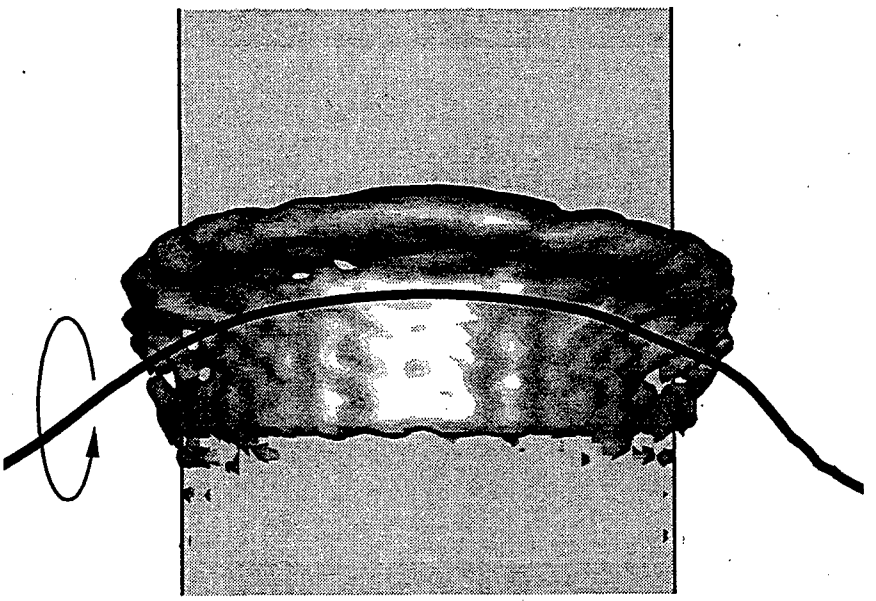

Fig. 22. Iso-surface of vorticity magnitude, showing the quasi two-dimensional ridge of secondary vorticity wrapping around the cylinder front, for the case with normal free-stream velocity [2].

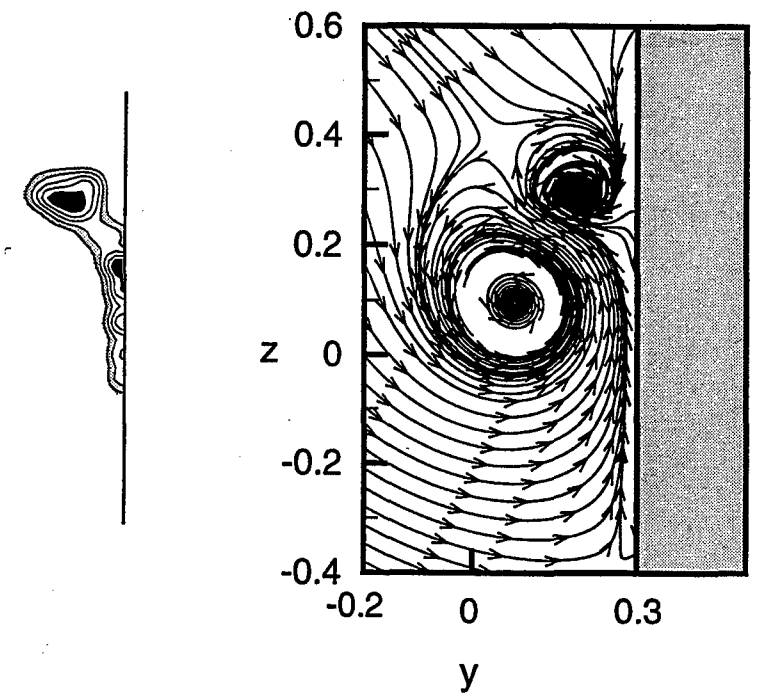

Fig. 23. Normal vorticity contour plot and streamlines over a slice of the secondary vortex structure in the *y*-*z* plane for the case with normal free-stream velocity [2].

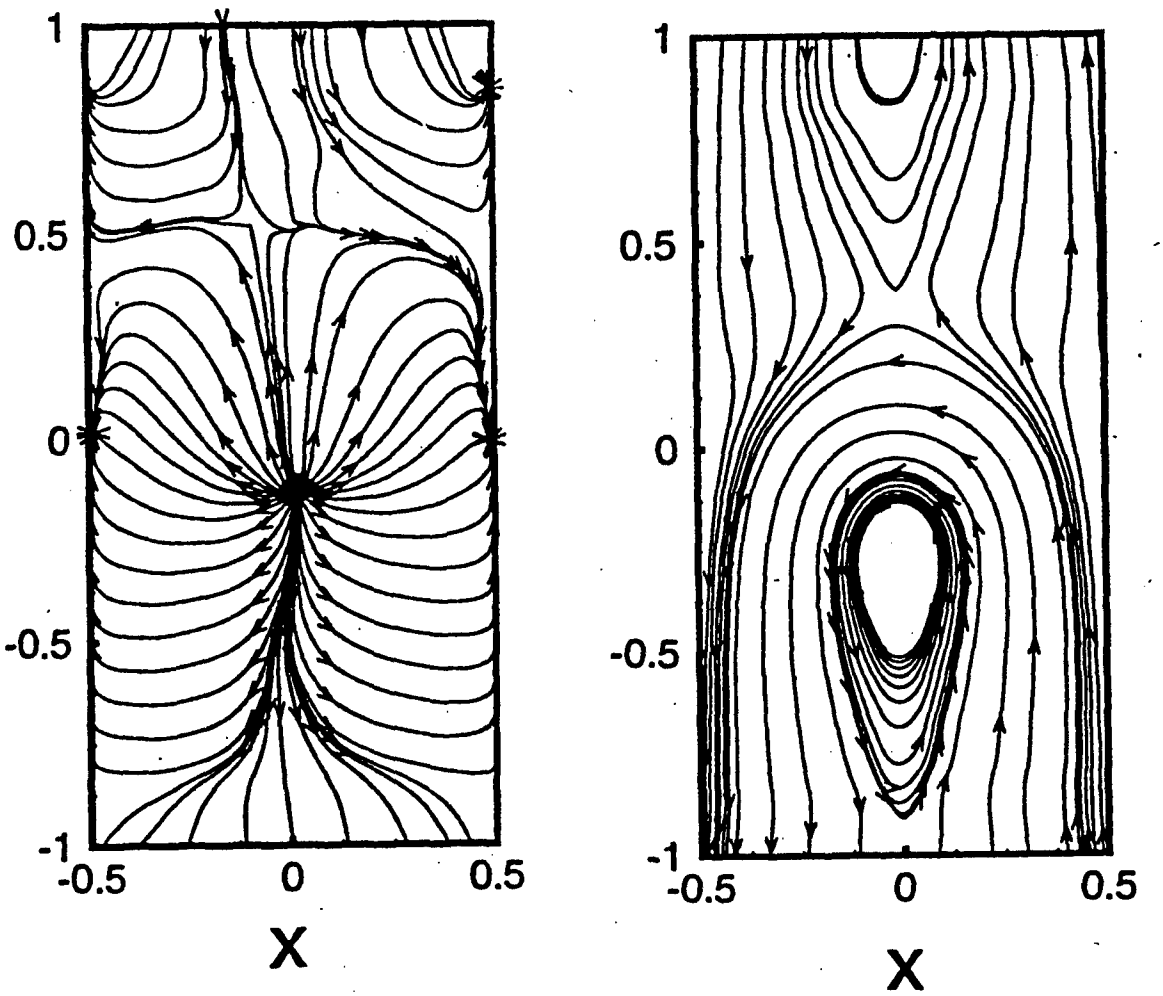

Fig. 24. Plot of the (a) limiting surface streamlines and (b) surface vortex lines for vortex-cylinder interaction with normal free-stream velocity [2].

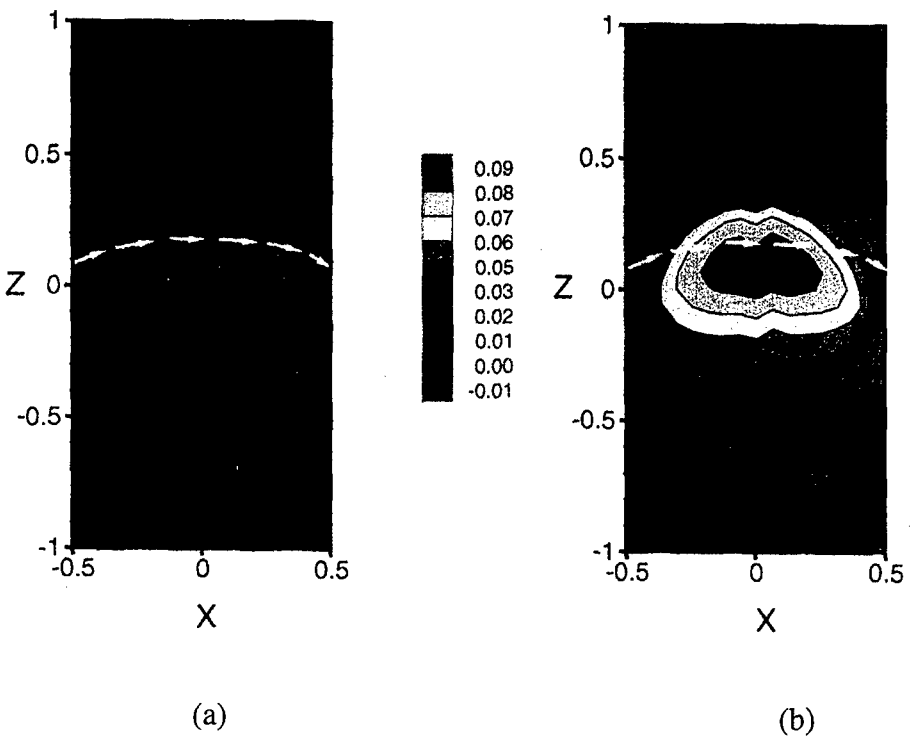

(a) (b)

Fig. 25. Surface pressure for vortex-cylinder interaction with (a) inviscid and (b) viscous flow for a case with normal free-stream velocity [2].

3. Conclusions and Future Work

The experimental research performed during this project is the most comprehensive study to date of the secondary vorticity shed during normal interaction between a columnar vortex and bodies of different shapes. The results of this study have lead to an understanding of the structural form of the secondary vorticity structures and of how the ejection and form of these structures is sensitive to the impact parameter *I*. A study was also performed showing that the inviscid vortex filament prediction becomes inaccurate shortly after secondary vorticity is ejected from the body. The study provided qualitative results which show that the secondary vortices can have a large effect on the primary vortex, which depending on the strength of the secondary vortex relative to the primary vortex may include formation of waves of variable core area on the primary vortex core, stripping of vorticity from the primary vortex, and sometimes even complete breakdown of the primary vortex, leading to disruption into small-scale turbulence.

The computational studies performed during this project have examined in detail the response of the primary vortex to wrapping of secondary vorticity structures and to abrupt cutting of the primary vortex by a thin body. Full Navier-Stokes computations of normal vortex-cylinder interaction have been performed which show that the form of the secondary vortex structure is quite different for cases with high and low impact parameter, in agreement with our experimental observations. These computations also show that the cylinder surface pressure is strongly effected by the secondary vorticity after it has been ejected from the body. Of particular note is the observation that very shortly after ejection, the secondary vorticity causes large changes to the velocity field external to the body boundary layer, even reversing the direction of flow tangent to the body surface in the region above the primary vortex. For this reason, simulations based on solution of the boundary layer equations (e.g., [1, 14]) will have very limited predictive capability after the secondary vorticity begins to be ejected from the body.

This project also resulted in the development and validation of a new computational method, which is generally applicable to three-dimensional viscous fluid flow past an immersed body. This method has all of the advantages of traditional vortex methods, and the particularly important advantage of no numerical dissipation, but it has the additional advantage of utilizing a continuous vorticity interpolation over anisotropic elements that do not penetrate into the body surface. Some aspects of the method are still being refined, involving improvement in efficiency and robustness for high Reynolds number flows.

However, in its current state the method is useful for low to moderate Reynolds number flows past three-dimensional bodies of arbitrary shape, and it is particularly well suited to computation of separated vortex flows in general and vortex-body interaction in particular due to the lack of numerical dissipation.

Future work should extend our study of secondary vorticity evolution in three-dimensional vortex-body interaction to parallel and perpendicular interactions with bodies of various types. Particularly, a full Navier-Stokes computation should be performed for the problem of penetration of a thin blade into a vortex with non-zero axial flow, to examine the effect of boundary layer separation from the body leading edge as it encountered the vortex axial flow during the initial penetration. Similarly, a more comprehensive investigation should be performed of the effect of free-stream velocity tangential to the cylinder axis on vortex-cylinder interaction, with comparison to experimental results. The effect of three-dimensionality on nearly parallel vortex-body interaction problems should also be investigated, particularly since slight three-dimensional perturbations of the vortex may dramatically change the structure of the secondary vorticity field. Finally, an exciting extension of this study would be to examine the effect on the secondary vorticity and body force caused by blowing or suction at the body surface. Such a study would lay the groundwork for active control of vortex-body interaction forces in future Army systems.

LIST OF PUBLICATIONS AND TECHNICAL REPORTS

The following publications have resulted from the research supported through this project.

A. Journal Papers and Book Chapters, In Press or Published

1. Marshall, J.S. and Beninati, L.M., "Turbulence Evolution in Vortex-Dominated Flows," *Advances in Fluid Mechanics*, Computational Mechanics Press, Southampton, UK (in press).

2. Krishnamoorthy, S., Gossler, A.A. and Marshall, J.S., "Normal Vortex Interaction With a Circular Cylinder," *AIAA Journal*, Vol. 37, No. 1, 1999, pp. 50-57.

3. Krishnamoorthy, S. and Marshall, J.S., "Three-Dimensional Blade-Vortex Interaction in the Strong-Vortex Regime," *Physics of Fluids*, Vol. 10, No. 11, 1998, pp. 2828-2845.

4. Marshall, J.S. and Grant, J.R., "A Lagrangian Vorticity Collocation Method for Viscous, Axisymmetric Flows With and Without Swirl," *Journal of Computational Physics*, Vol. 138, 1997, pp. 302-330.

5. Marshall, J.S. and Krishnamoorthy, S., "On the Instantaneous Cutting of a Columnar Vortex With Non-Zero Axial Flow," *Journal of Fluid Mechanics*, Vol. 351, 1997, pp. 41-74.

6. Marshall, J.S., "The Flow Induced By Periodic Vortex Rings Wrapped Around a Columnar Vortex Core," *Journal of Fluid Mechanics*, Vol. 345, 1997, pp. 1-30.

7. Marshall, J.S. and Chen, H., "Stability of a Counter-Rotating Vortex Pair Immersed in a Cross-Stream Shear Flow," *AIAA Journal*, Vol. 35, No. 2, 1997, pp. 295-305.

8. Marshall, J.S. and Grant, J.R., "A Method for Determining the Velocity Induced By Highly Anisotropic Vorticity Blobs," *Journal of Computational Physics*, Vol. 126, No. 2, 1996, pp. 286-298.

B. Journal Papers, Submitted or In Preparation

1. Gossler, A.A. and Marshall, J.S., "Simulation of Normal Vortex-Cylinder Interaction in a Viscous Fluid," *Journal of Fluid Mechanics* (submitted).

2. Marshall, J.S., Grant, J.R., Gossler, A.A. and Huyer, S.A., "Vorticity Transport on a Lagrangian Tetrahedral Mesh," *Journal of Computational Physics* (submitted).

3. Sun, M. and Marshall, J.S., "Vortex Interaction With the Wake of a Sphere," *Journal of Fluid Mechanics* (submitted).

C. Conference Papers

1. Marshall, J.S., "Response of a Columnar Vortex to a Wrapped Vortex Loop," Third International Workshop on Vortex Flows and Related Numerical Methods, Toulouse, France, Aug. 24-27, 1998 (to be published in *European Series in Applied and Industrial Mathematics*).

2. Grant, J.R. and Marshall, J.S., "Inviscid Interaction of Vortex Rings: Approach to Singularity," Third International Workshop on Vortex Flows and Related Numerical Methods, Toulouse, France, Aug. 24-27, 1998 (to be published in *European Series in Applied and Industrial Mathematics*).

3. Gossler, A.A., Marshall, J.S. and Grant, J.R., "Vorticity-Based Simulation of Vortex-Body Interaction," 51st Meeting of the Fluid Dynamics Division of the American Physical Society, Philadelphia, Penn., Nov. 22-24, 1998 (*Bulletin of the American Physical Society*, Vol. 43, No. 9, p. 1992).

4. Marshall, J.S. and Krishnamoorthy, S., "Three-Dimensional Vortex-Body Interaction in a Viscous Fluid," *Symposium on Separated and Complex Flows*, ASME Fluids Engineering Division Summer Meeting, Vancouver, B.C., June 22-26, 1997.

D. Technical Reports

1. Marshall, J.S., "Three-Dimensional Vortex-Body Interaction in a Viscous Fluid," Final report for ARO grant DAAH04-96-1-0081, 1999.

E. Theses and Dissertations

1. Gossler, Albert, "A Tetrahedral Element Lagrangian Vorticity Method With Application to Vortex-Cylinder Interaction," Ph.D. dissertation, The University of Iowa, Iowa City, July, 1999.

2. Krishnamoorthy, Srikanth, "Normal Vortex-Body Interaction in a Three-Dimensional Viscous Flow," Ph.D. dissertation, The University of Iowa, Iowa City, December, 1997.

3. Sun, Meihong, "A Study of Vortex Interaction With a Sphere Wake," M.S. thesis, The University of Iowa, Iowa City, June, 1998.

LIST OF PARTICIPATING SCIENTIFIC PERSONNEL

Dr. Jeffrey S. Marshall, Associate Professor, Principal Investigtor

Dr. Srikanth Krishnamoorthy, Ph.D. level graduate research assistant, Ph.D. awarded Dec. 1997 by The University of Iowa

Ms. Meihong Sun, M.S. level graduate research assistant, M.S. awarded June 1998 by The University of Iowa

Dr. Albert Gossler, Ph.D. level graduate research assistant, Ph.D. awarded July 1999 by The University of Iowa (supported under AASERT augmentation award for this project)

REPORT OF INVENTIONS

The following U.S. patent was received during the course of this project. This patent was filed by the Department of the Navy for work on computational algorithm development performed in collaboration with investigators at the Naval Undersea Warfare Center, Newport, Rhode Island:

J.R. Grant, S.A. Huyer, J.S. Uhlman, and J.S. Marshall, "Algorithms and Code for Computing Three-Dimensional Unsteady Flow By Solution of the Vorticity Equation on a Lagrangian Mesh", U.S. Patent.

REFERENCES

1. Affes, H., Xiao, Z. and Conlisk, A.T., "The Boundary Layer Flow Due to a Vortex Approaching a Cylinder," *J. Fluid Mech.*, Vol. 275, 1994, pp. 33-57.

2. Gossler, A.A. and Marshall, J.S., "Simulation of Normal Vortex-Cylinder Interaction in a Viscous Fluid," *J. Fluid Mech.* (submitted).

3. Krishnamoorthy, S., Gossler, A.A. and Marshall, J.S., "Normal Vortex Interaction With a Circular Cylinder," *AIAA J.*, Vol. 37, No. 1, 1999, pp. 50-57.

4. Krishnamoorthy, S. and Marshall, J.S., "An Experimental Investigation of 'Vortex Shocks'," *Phys. Fluids*, Vol. 6, No. 11, 1994, pp. 3737-3741.

5. Krishnamoorthy, S. and Marshall, J.S., "Three-Dimensional Blade-Vortex Interaction in the Strong-Vortex Regime," *Phys. Fluids*, Vol. 10, No. 11, 1998, pp. 2828-2845.

6. Lee, J., Burggraf, O.R. and Conlisk, A.T., "On the Impulsive Blocking of a Vortex-Jet," *J. Fluid Mech.*, Vol. 369, 1998, 301-331.

7. Lundgren, T.S. and Ashurst, W.T., "Area-Varying Waves on Curved Vortex Tubes with Application to Vortex Breakdown," *J. Fluid Mech.*, Vol. 200, 1989, pp. 283-307.

8. Marshall, J.S., "Vortex Cutting by a Blade. Part I. General Theory and a Simple Solution," *AIAA J.*, Vol. 32, No. 6, 1994, pp. 1145-1150.

9. Marshall, J.S., "The Flow Induced By Periodic Vortex Rings Wrapped Around a Columnar Vortex Core," *J. Fluid Mech.*, Vol. 345, 1997, pp. 1-30.

10. Marshall, J.S. and Krishnamoorthy, S., "On the Instantaneous Cutting of a Columnar Vortex With Non-Zero Axial Flow," *J. Fluid Mech.*, Vol. 351, 1997, pp. 41-74.

11. Marshall, J.S. and Grant, J.R., "Penetration of a Blade Into a Vortex Core: Vorticity Response and Unsteady Blade Forces," *J. Fluid Mech.*, Vol. 306, 1996, pp. 83-109.

12. Maxworthy, T., Hopfinger, E.J. and Redekopp, L.G., "Wave Motions on Vortex Cores," *J. Fluid Mech.*, Vol. 151, 1985, pp. 141-165.

13. Sarpkaya, T. and Daly, J.J., "Effect of Ambient Turbulence on Trailing Vortices," *J. Aircraft*, Vol. 24, 1987, pp. 399-404.

14. Xiao, Z., Burggraf, O.R. and Conlisk, A.T., "The Interacting Boundary-Layer Flow Due to a Vortex Approaching a Cylinder," *J. Fluid Mech.*, Vol. 346, 1997, pp. 319-343.